The Radiation Instability of Thermally Stable Nanocrystalline Platinum-Gold

Ryan Schoell[a], Christopher M. Barr[a], Douglas L. Medlin[b], David P. Adams[a], Yasir Mahmood[c], Fadi Abdeljawad[c,d,e], and Khalid Hattar[a,f,*]

[a] *Material, Physical, and Chemical Sciences Center, Sandia National Laboratories, Albuquerque, USA*

[b] *Energy Nanomaterials Department, Sandia National Laboratories, Livermore, United States*

[c] *Department of Mechanical Engineering, Clemson University, Clemson, South Carolina 29634, United States*

[d] *Department of Materials Science and Engineering, Clemson University, Clemson, South Carolina 29634, United States*

[e] *Department of Materials Science and Engineering, Lehigh University, Bethlehem, PA, United States*

[f] *Department of Nuclear Engineering, University of Tennessee – Knoxville, Knoxville, TN, United States*

*khattar@utk.edu

Recent experimentally validated alloy design theories have demonstrated nanocrystalline binary alloys that are stable against thermally induced grain growth. An open question is whether such thermal stability also translates to stability under irradiation. In this study, we investigate the response to heavy ion-irradiation of a nanocrystalline platinum-gold alloy that is known to be thermally stable from previous studies. Heavy ion-irradiation was conducted at both room temperature and elevated temperatures on films of nanocrystalline platinum and platinum-gold. Using scanning/transmission electron microscopy equipped with energy dispersive spectroscopy and automated crystallographic orientation mapping, we observe substantial grain growth in the irradiated area compared to the controlled area beyond the range of heavy ions, as well as compositional redistribution under these conditions and discuss mechanisms underpinning this instability. These findings highlight that grain boundary stability against one external stimulus, such as heat, does not always translate into grain boundary stability under other stimuli, such as displacement damage.

Keywords: Nanocrystalline, Binary Alloy, Thermal Stability, Radiation Stability

Introduction

Grain growth in metals can be induced by a variety of driving forces with the three most common stimuli being thermal exposure, mechanical loading, and irradiation [1, 2]. The far-from-equilibrium and large interconnected network of grain boundaries in nanocrystalline metals results in materials that are microstructurally unstable (i.e., exhibiting rampant grain growth under different environmental exposures) and for which mechanisms underpinning stability are still highly debated [1, 3-7]. In response, much recent research has sought to hinder grain growth and thereby to limit the inherent instability resulting from high interfacial density [8-12] by alloying. Based on both experimental and theoretical analyses, it has been proposed that the segregation of solutes either stagnates grain growth via solute drag [12] or that it stabilizes the grain boundaries by reducing interfacial free energy, i.e., the thermodynamic route, and thus lowering the driving force for growth [9, 12]. However, an open question is whether the mechanisms that stabilize grain boundaries to thermal stressors will also operate in the same manner under irradiation. Indeed, given that irradiation has been shown to drive grain growth in several systems [2, 13-15], it is quite possible that it could counteract the stability mechanisms provided by alloying. Competing mechanisms like radiation-induced mixing and thermal diffusion of solutes to boundaries from the bulk would dictate the ability for the grains to grow and higher temperatures could prove to overcome radiation-induced mixing.

The thermodynamic route to the stability of nanocrystalline materials has emerged from early models including those by Murdoch et al. [8] and Trelewicz et al. [9] that replaced empirical equations based on size mismatch, low bulk solubility, and cohesive energy with a model related to the enthalpy of mixing and segregation [16-18]. Recent approaches include those suggested by

Rupert et al. [11], who observed Amorphous Intergranular Films (AIF) at grain boundaries of some binary metallic alloys and developed selection rules for AIF formation based on the enthalpy of mixing, enthalpy of segregation, and the atomic radius mismatch. Other models developed by VanLeeuwen et al. [12] showed that the chemical contribution must be taken into account along with elastic strain energy to estimate the reduction in the thermodynamic driving force for grain growth. Mechanically-driven grain growth has been thought to either be the result of stress [6, 19] or strain [5]. Alloy design to mitigate grain growth from irradiation has been sparse [20-22]. Irradiation of nanocrystalline materials has been found to cause grain growth via thermal spikes [15] where atomic jumps within a thermal spike, defined here as the thermal energy created during a single cascade event, leads to boundary migration. Moreover, the model includes cascade and sub-cascade structures at grain boundaries [15]. Recent models have attempted to add the role of grain boundary character in irradiation induced grain growth [23]. Some studies have been conducted to examine the effects of ion beam mixing on different phases to study their stability, especially in immiscible binary alloys [24-26]. Further experimentation to evaluate potential stability of nanocrystalline alloys under irradiation needs to be conducted to develop an understanding of the mechanisms of grain size stability.

In this study, we investigate the potential competing effects active from both thermal and heavy ion-irradiation on grain growth. We focus on the Pt-10Au system, an alloy system for which solute segregation to the grain boundaries is well known to stabilize the material against thermal grain growth [27-30]. We also discuss these findings in the context of other stressors, such as mechanical loading. Specifically, this study shows how optimization against one external stimulus does not equate to stabilization against other stimuli.

Materials and Methods

Two films were grown via direct current magnetron sputtering to create 5 μm of pure Pt and Pt-10 at. %Au (Here on out referred to as Pt-10Au) on a thermally oxidized (100) oriented Si substrate with a 400 nm SiO_2 layer using targets with 99.99 at.% purity. The composition of the films was determined using a JEOL model JXA-8530F Wavelength Dispersive Spectroscopy operating at 7 kV with a compositional resolution of 0.5 at.% [29]. Pt and Pt-10Au were specifically selected to decouple the effects of segregation on the stability of the microstructure due to both thermal and irradiation stressors. Moreover, the nanocrystalline Pt-10Au system is known to be stable against grain growth under thermal exposure due to segregation of Au to the grain boundaries [27-30], and thus it serves as a well understood system for exploring the still nebulous effects of irradiation. The Pt-10Au on Si was heat treated in a vacuum furnace at 500 °C for 2 hours to induce gold segregation to the grain boundaries in the Pt-10Au sample based on the results of a previous study on this system [27]. Sections of both films were then irradiated with 20 MeV Au^{4+} at nominally room temperature and at 500 °C to a total fluence of 2×10^{16} ions cm^{-2} to a peak damage of ~140 displacements per atom (dpa) according to the Stopping and Range of Ions in Matter (SRIM) 2008 software (Displacement energy set to 40 eV for both Au and Pt) [31]. The film thickness and ion irradiation energy were specifically chosen to irradiate half the 5 μm-thick film so that an irradiated region could be directly compared to the vicinal non-irradiate region below and any surface effects could be minimized. The ion species of Au was chosen because heavy ion irradiation was desired and self-ion irradiation for the Pt-Au system would remove the effects of other elemental species even with low implanted atomic concentrations on the order of 10^{-3} at%. In fact, the general columnar nature of the sputter deposited microstructure provides a means of having the same grains in both the irradiated region and the non-irradiated region for

comparison.

TEM specimens containing both irradiated and non-irradiated regions were prepared by Focused Ion Beam (FIB) techniques using a Thermo Fisher Scientific Scios 2 Dual Beam system. Initial trenches were created using a 30 kV 15 nA gallium beam far from the desired sample location and sequentially lower beam energy and currents were used closer to the sample. The specimens were finished with a final 2 kV polish step to reduce the amount of FIB induced damage to the sample. The non-irradiated microstructures were obtained from regions beyond both the damage profile and implanted gold profile created by the ion irradiation. Bright-Field (BF) micrographs were collected via an image-corrected FEI Titan Transmission Electron Microscope (TEM) operating at 300 kV. Grain sizes were measured and analysed in both irradiated and non-irradiated regions via an ASTM E112-13 linear intercept method. Chemical mapping was conducted by Energy Dispersive X-ray Spectroscopy (EDS) in probe corrected scanning transmission electron microscope (FEI ThemisZ operated at 300 kV). EDS quantification was conducted using the Thermo Fisher Velox Software, using library reference standards. Both instruments are equipped with 4-quadrant EDS detectors. Automated Crystallographic Orientation Mapping (ACOM) was performed on a JEOL 2100 TEM operated at 200 kV.

Results

As is common (or typical) of FCC films grown by physical vapor deposition, both the Pt and Pt-10Au films grew in a predominately (111) orientated with columnar structures thus making the films equiaxed in plan-view and columnar in cross section. The thermal stability of these Pt and Pt-Au alloys over a range of Au concentrations has been extensively studied in multiple previously reported plan-view *in situ* TEM experiments [27-30].

Figure 1a and b show FIB lift-outs of the Pt film after irradiation at room temperature in the non-irradiated region and the irradiated region, respectively. Similarly, the BF TEM micrographs associated with the non-irradiated and irradiated regions of the Pt-10Au sample after room temperature irradiation are shown in Figure 1c and d. In both films, extensive grain growth occurred within the irradiated region with an average grain size and a standard deviation of 190 ± 69 nm and 160 ± 82 nm in the Pt and Pt-10Au samples, respectively. In contrast, the non-irradiated region showed average grain sizes and standard deviation of 52 ± 17 nm and 57 ± 21 nm in the Pt and Pt-10Au samples, respectively. The grain size distributions for both the irradiated and non-irradiated regions are shown in Figure 1e in both the Pt and Pt-10Au films. Since these grains are columnar, the grain width is sufficient to describe the grain size, and this is what is represented in figure 1e.

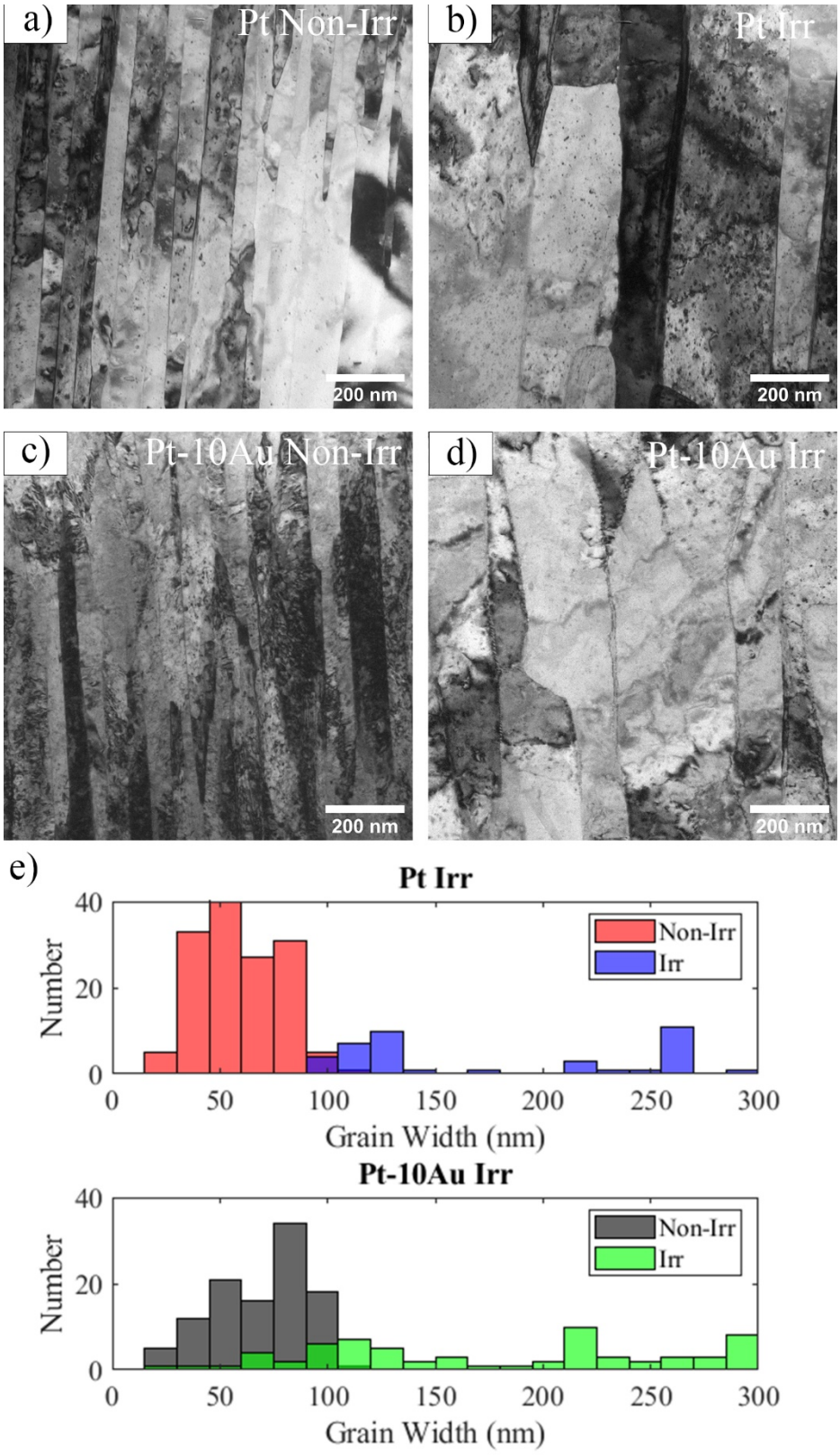
a)
Pt Non-Irr
200 nm
b)
Pt Irr
200 nm
c)
Pt-10Au Non-Irr
200 nm
d)
Pt-10Au Irr
200 nm
e)
Pt Irr
Non-Irr
Irr
Number
Grain Width (nm)
Pt-10Au Irr
Non-Irr
Irr
Number
Grain Width (nm)

Fig. 1. BF TEM of irradiated room temperature Pt in (a) non-irradiated and (b) irradiated region and Pt-10Au in (c) non-irradiated and (d) irradiated region. Histograms of grain width in irradiated and non-irradiated regions in the (e) Pt and (f) Pt-10Au samples.

In contrast to the behaviour of the films under purely thermal exposure, the Pt-10Au films are unstable to radiation-induced grain growth. A High Angle Annular Dark-Field (HAADF) STEM micrograph of the resulting microstructure after ion irradiation is shown in Figure 2. Comparing the simulated damage profile, computed using SRIM [31], with the HAADF micrograph shows a clear division between the irradiated regions with large grain sizes and the non-irradiated region with smaller grain sizes. It is also interesting to compare the distribution of Au, as measured by EDS. In the unirradiated region, Au is segregated to the grain boundaries, consistent with previous reports [27-30]. In contrast, the irradiated region of the adjacent microstructure has grain boundaries that are no longer enriched in Au.

Pores of about 18 nm ± 5 nm were also identified in the irradiated region at the grain boundaries. We hypothesize that these most likely arise from the clustering of vacancies already present in the as-deposited film microstructure and vacancies introduced through irradiation mechanisms. The presence of these voids highlights the high concentrations of vacancies that irradiation induces in the irradiated region. Similar voids have been experimentally observed previously in this system [28, 32]

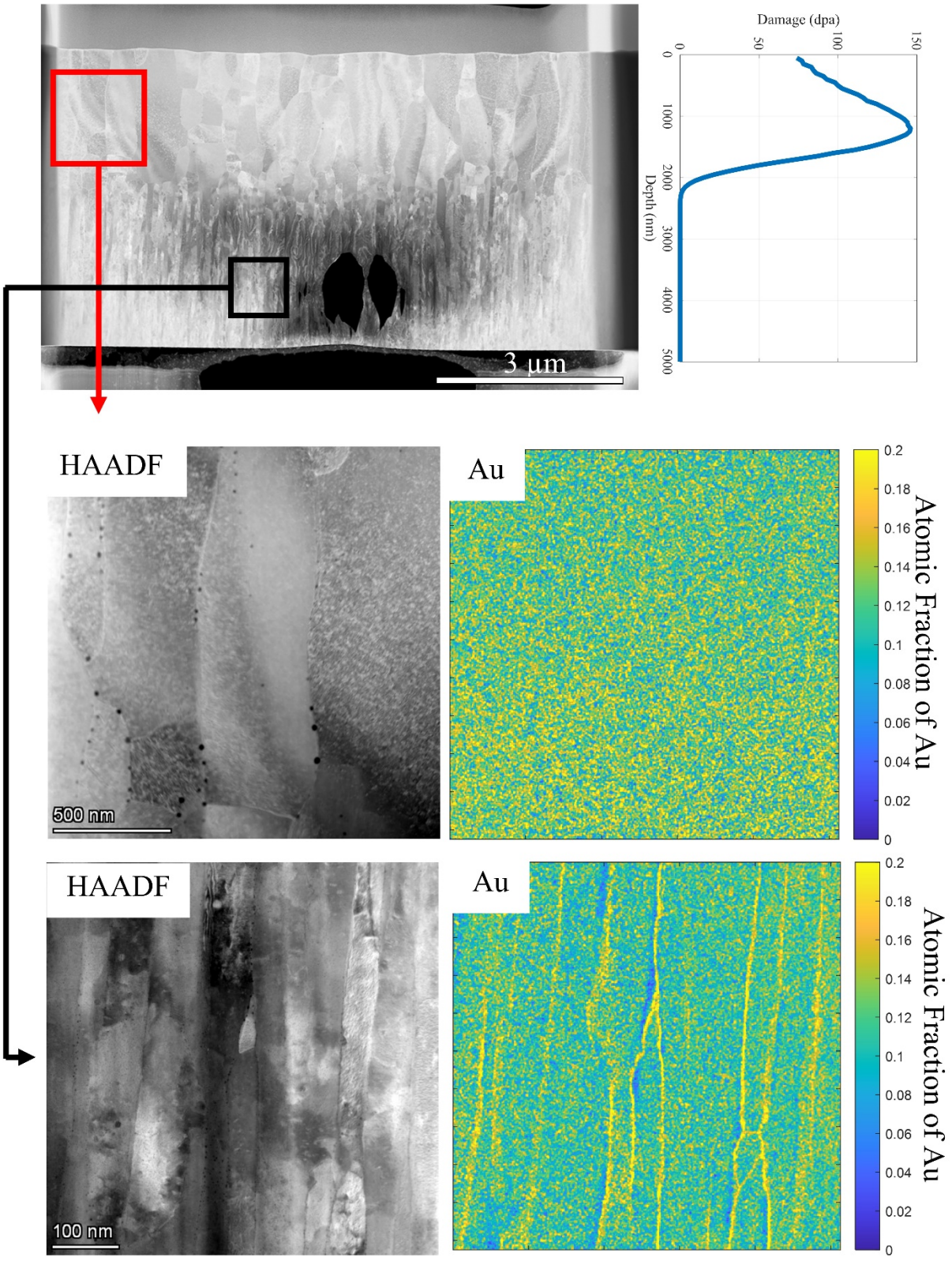

Fig. 2. HAADF STEM micrograph of Pt-10Au film after 20 MeV Au^{4+} ion irradiation at room temperature to a fluence of 2×10^{16} ions cm^{-2} and elemental maps of Au.

A similar analysis was done on the samples irradiated at 500 °C using the 20 MeV Au^{4+} ion beam. Figure 3 shows the BF micrographs associated with the irradiated and non-irradiated regions of Pt and Pt-10Au after irradiation at 500 °C. Like the room temperature irradiations, extensive grain growth, compared to the non-irradiated region, is evident within the irradiated region in both the Pt and Pt-10Au samples. Further analysis of the Pt-10Au sample irradiated at 500 °C showed desegregation of Au that is still present in the non-irradiated region as shown in Figure 4.

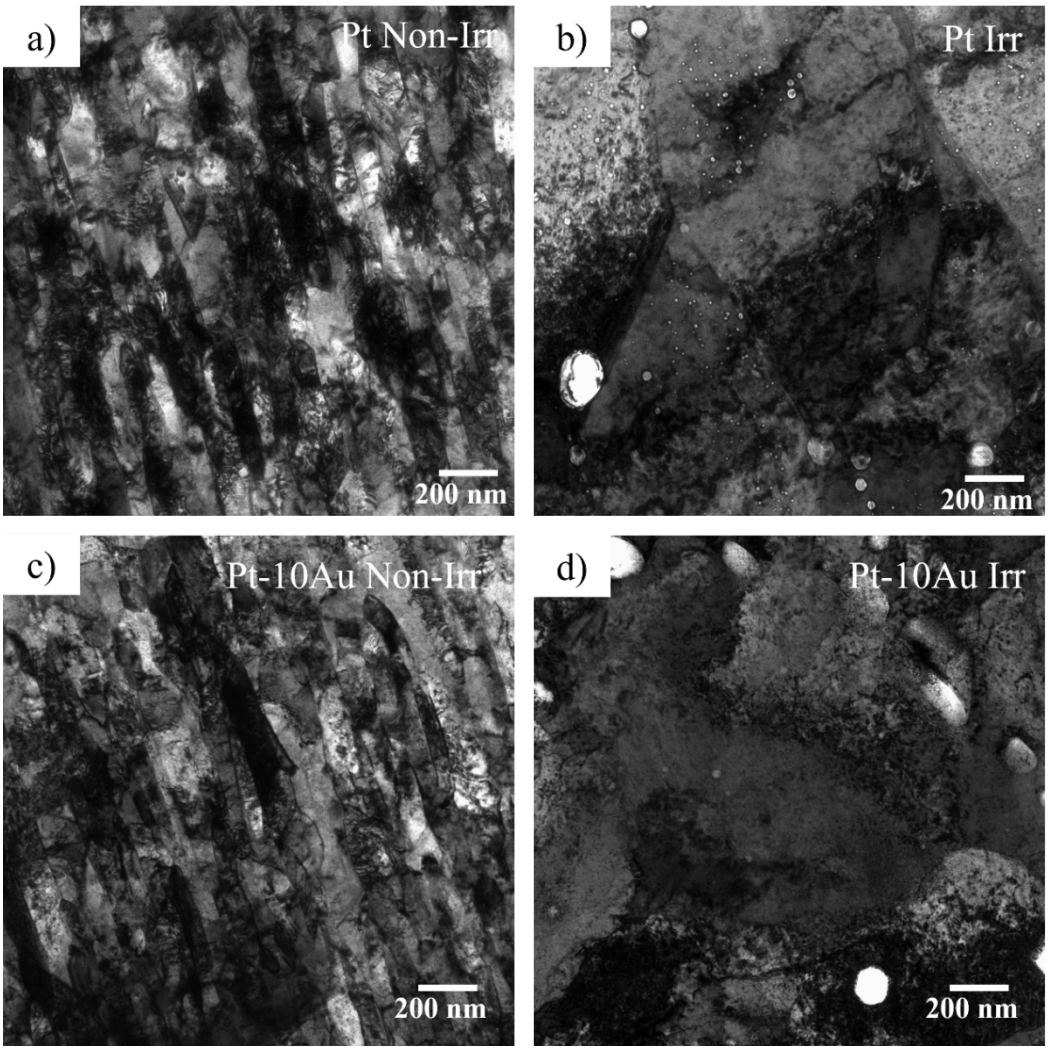

Fig. 3. BF TEM of irradiated 500 °C Pt in (a) non-irradiated and (b) irradiated region and Pt-10Au in (c) non-irradiated and (d) irradiated region.

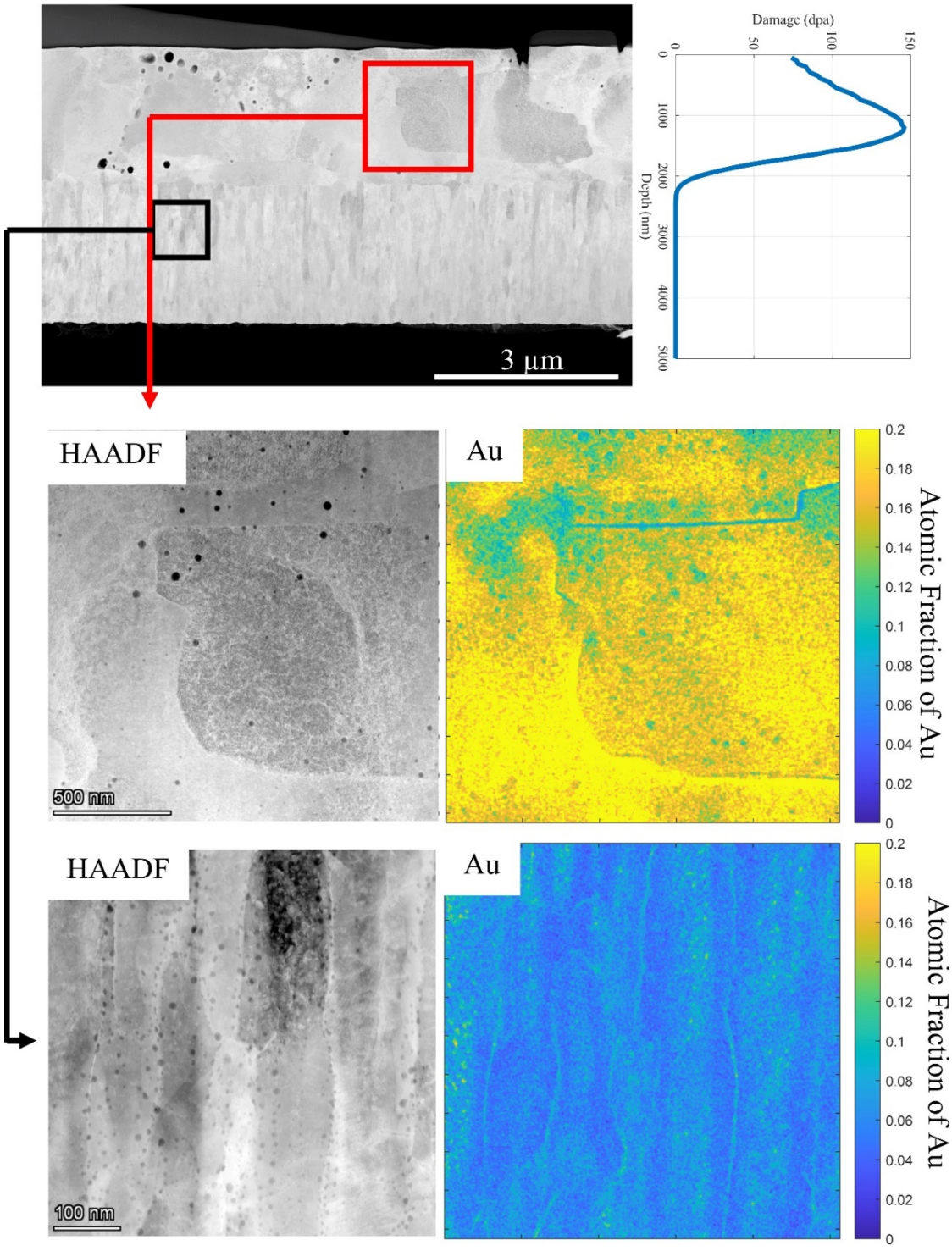

Fig. 4. HAADF STEM micrograph and Au compositional maps of Pt-10Au film after 20 MeV Au^{4+} ion irradiation at 500 °C to a fluence of 2×10^{16} ions cm^{-2}

We also analyzed the changes in the grain structure and orientations with the aim of determining which boundary misorientations were more prevalent. Figure 5 shows the results of the ACOM mapping in both the room temperature (Figure 6a) and 500 °C samples (Figure 6b), indicating that that higher angle grain boundaries (>30°) are more prevalent in the irradiated region compared to the non-irradiated region as is depicted in the bar graph Figure 6c indicating the preferential removal of low angle grain boundaries during the grain growth process.

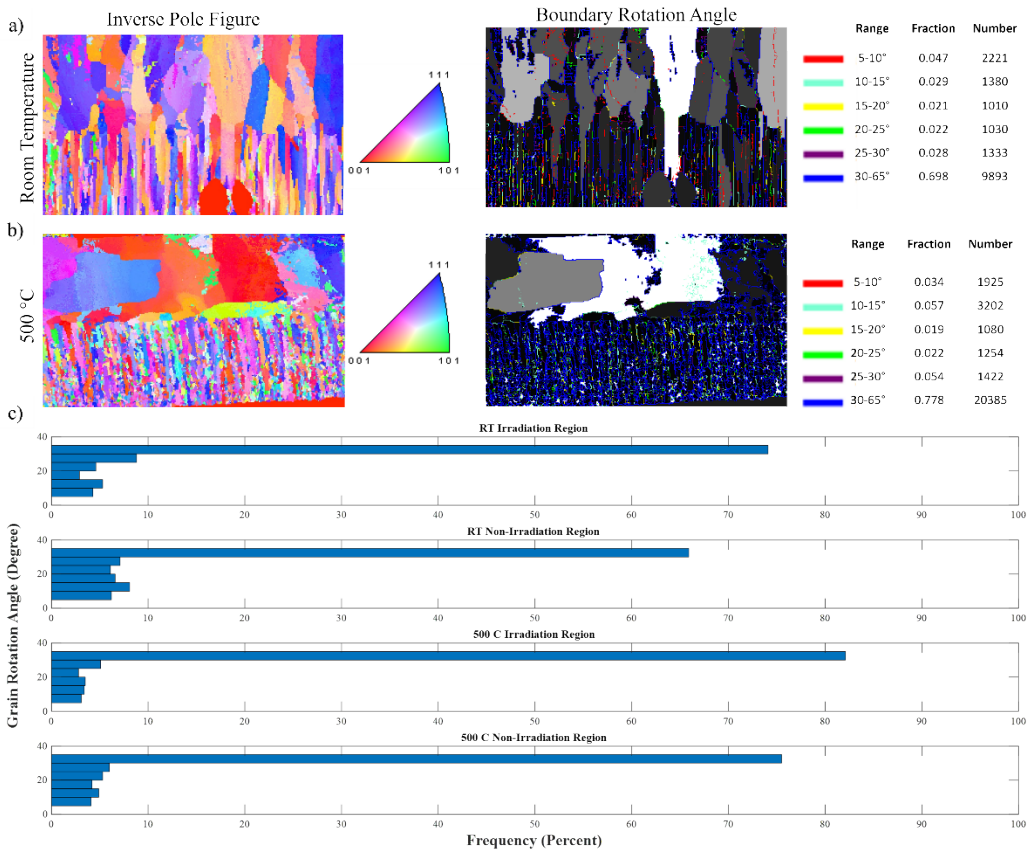

Fig. 5. ACOM of Pt-10Au films at (a) room temperature and (b) 500 °C with (c) histogram of grain boundaries.

Beyond specifically looking at segregation of Au at grain boundaries and their misorientation, Figure 6 shows compositional measurements across the entire thickness of the films (i.e., along the deposition direction) for both the room temperature and 500 °C condition. Enrichment of the Au/Pt ratio in the irradiated region of the 500 °C specimen can be seen.

Analysis of line scan profiles indicates that the Au concentration has increased to approximately 15 at.% in the upper irradiated region and decreased to approximately 5 at.% in the lower, unirradiated region.

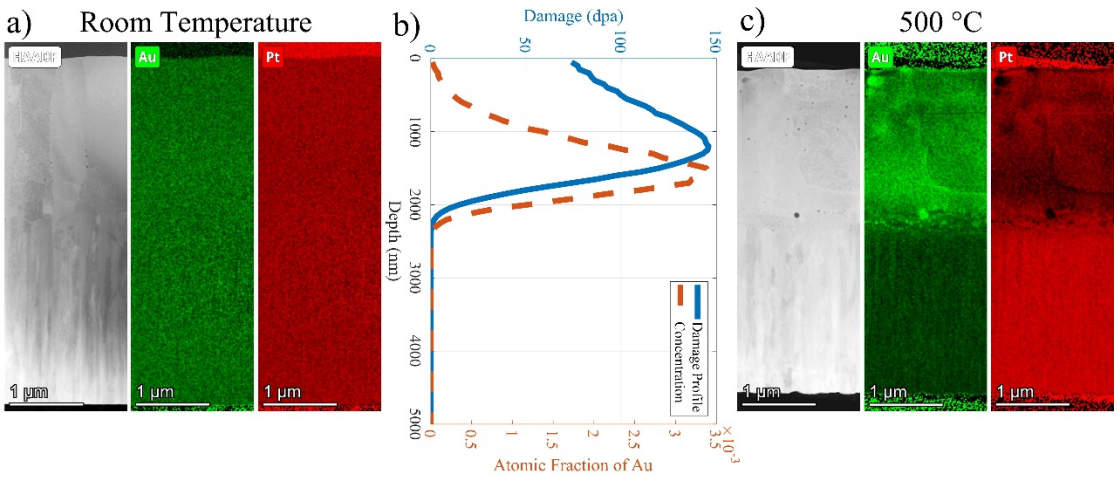

Fig. 6. a) HAADF and elemental maps of the room temperature sample showing both irradiated and pristine regions. b) SRIM simulation with both the damage profile and concentration of implanted Au plotted for the Pt-10Au samples at a fluence of 2×10^{16} ions cm^{-2}. c) HAADF and elemental maps of the 500 °C sample over the thickness of the film showing strong Au segregation to the irradiated region

Discussion

Previous studies on the Pt-10Au system [28, 30] have revealed the stability of nanocrystalline microstructure at elevated temperatures of 500 °C and 700 °C compared to pure nanocrystalline Pt. The stability of Pt-10Au system has been associated with Au segregation to the Pt grain boundaries reducing the energy of the boundary and therefore reducing the driving force for grain growth [28, 30]. In previous experimental work, STEM EDS maps of films annealed at 500 °C revealed that the segregation of Au to the grain boundaries is heterogeneous and depends on grain boundary type: at low angle grain boundaries Au concentration ranged from 17-22 at.%, at high angle grain boundaries the concentration ranged from 30-45 at.%, whereas coherent twin

boundaries showed no discernible segregation [30]. Previous reports suggest only a subset of the grain boundary segregation is needed to maintain a nanocrystalline microstructure under thermal conditions [33]. Although previous studies have demonstrated that the Pt-10Au system shows some stability against grain growth under thermal conditions [28, 30], our findings here show that this system is unstable to grain growth under irradiation, both at room temperature and at elevated temperature. Irradiation led to a higher frequency of high angle grain boundaries that would have been suitable for Au stabilization at the boundaries [30]. This experiment illustrates how different stressors can have competing effects due to different operating mechanisms and that irradiation appears dominant at temperatures up to at least 500 °C.

Insight concerning the destabilizing effect of the heavy ion irradiation is provided by the observed absence of Au grain boundary segregation in the irradiated region. The experiments showed a lack of Au at the grain boundaries in the irradiated region. Ion beam mixing during heavy ion-irradiation could drive desegregation of Au at the boundaries and thus remove the stabilizing effects of the segregated Au. Irradiation has often been shown to have the opposite thermal solute effect, i.e., inverse Kirkendall and non-equilibrium mixing, compared to thermal effects [34]. Ion beam mixing can lead to the forced displacement of atoms, which competes with the thermally activated jumps and leads to non-equilibrium phase mixing [24]. Without the Au to stabilize the grain boundaries, ion-induced grain growth, as described by the thermal spike model [23], can occur.

Interestingly, the irradiation of the Pt-10Au sample at 500 °C did not show much reduction of grain growth. 500 °C, ~0.3 T_m, was chosen to provide adequate mobility to the solute, vacancies, and interstitials without having thermally dominated processes govern the microstructural evolution. Although the entropic effect at elevated temperatures is expected to reduce grain

boundary segregation effects, the results indicated that the effects of irradiation were more dominant than the Au segregation effects, i.e., equilibrium grain boundary segregation. The Au solute demonstrated extensive long-range diffusion, no preferential accumulation at grain boundaries, and more grain growth than either the sample just heated to 500 °C or irradiated under the same condition but at nominally room temperature. Effects from ion beam heating are ruled out since irradiation was done at 500 °C and therefore well above the expected temperature increase due to beam heating of conductive metals with 20 MeV and a current on the order of 10 nA [35]. The other mechanism which might be at play would be one where excess interstitials and vacancies at the grain boundary as a result of irradiation cause migration of slower smooth boundaries that would otherwise inhibit grain growth [33]. As such, it is now hypothesized that ion beam mixing can simultaneously lead to the forced displacement of Au, cause significant migration of Au from the grain boundaries, and alter the grain boundary character--which can all contribute to the grain growth observed. Further work is needed to deconvolute the potential contributions of each.

As noted above, we also observed a redistribution of solute, enriching the Au concentration in the irradiated region of the 500 °C sample compared to the relatively homogeneous overall Au concentration in the room temperature sample (see Figure 6). While this observation is not the primary focus of this study, it is useful to briefly consider the factors controlling this redistribution. Our goal is not to provide a mechanistic understanding of this solute redistribution, but rather illustrate a framework based on irreversible thermodynamics to quantitatively describe the observations in Figure 6. The irradiated region of the sample is characterized by a high density of point defects (i.e., vacancies and interstitials) compared to the pristine portion deeper than the end of range of the implanted damage. This in turn creates gradients in point defect concentrations

across the sample thickness. In such substitutional alloys, the flux of point defects down the sample thickness is accompanied by a flux of chemical species in the opposite direct. This mass transport is characterized by several transport coefficients, which are thermally activated, and the higher temperature leads to faster diffusion of species. We can eliminate ion-implantation as the source of the increased Au in the upper region of the 500 °C specimen for the following reasons. (1) This increase is not observed in the room temperature sample, and (2) the additional concentration due to implantation, as predicted by SRIM, is maximum around 0.35 at.%. In addition, the columnar structure can provide a faster diffusion path along the grain boundaries from the non-irradiated region to the irradiated region.

Irreversible thermodynamics provides a framework to model and quantify the various operative transport mechanisms. In addition to Pt and Au, Pt-Au alloys under irradiation are characterized by points defects, namely interstitials *i* and vacancies *v*. As a result, these systems can be described by four compositions fields, x_{pt}, x_{au}, x_i, and x_v for Pt, Au, interstitials, and vacancies, respectively. Following the treatment of Piochaud et al. [36], the fluxes of species j_α are related to driving force F_β as $j_\alpha = L_{\alpha\beta}F_\beta$, where $L_{\alpha\beta}$ are the Onsager transport coefficients. Using the Gibbs-Duhem relation $x_{pt}\nabla\mu_{pt} + x_{au}\nabla\mu_{au} = 0$ in the limit of dilute defect concentrations (i.e., $x_i \ll 1$ and $x_v \ll 1$) yields the following expression for the flux of Pt and Au species.

$$j_{pt} = -\left[\left\{\left(L^i_{pt,au} + L^v_{pt,au}\right)x_{pt} - \left(L^i_{pt,pt} + L^v_{pt,pt}\right)x_{au}\right\}\nabla\tilde{\mu} + \left(L^i_{pt,pt} + L^i_{pt,au}\right)\nabla\mu_i - \left(L^v_{pt,pt} + L^v_{pt,au}\right)\nabla\mu_v\right],$$

$$j_{au} = -\left[\left\{\left(L^i_{au,au} + L^v_{au,au}\right)x_{pt} - \left(L^i_{au,pt} + L^v_{au,pt}\right)x_{au}\right\}\nabla\tilde{\mu} + \left(L^i_{au,pt} + L^i_{au,au}\right)\nabla\mu_i - \left(L^v_{au,pt} + L^v_{au,au}\right)\nabla\mu_v\right],$$

where $\tilde{\mu} = \mu_{pt} - \mu_{au}$ is the chemical potential difference between Pt and Au. Here, transport in the Pt-Au alloy is assumed to be vacancy (i.e., $L^{v}_{\alpha\beta}$) and interstitial (i.e., $L^{i}_{\alpha\beta}$) mediated. The above expressions for Pt and Au fluxes highlight the complex transport mechanisms pathways that are operative during irradiation. For example, the flux of Au is governed by several transport coefficients $L^{i}_{au,au}$, $L^{v}_{au,au}$, $L^{i}_{au,pt}$, and $L^{v}_{au,pt}$, all of which are concentration and temperature dependent. Therefore, an understanding of solute redistribution shown in Figure 6 requires a detailed investigation of the various operative mass transport coefficients, including cross-diffusion terms, i.e., $L_{pt,\,au}$. The flux equations discussed above reveal the complex nature of defect-mediated mass transport processes in irradiated alloys and highlight the need to quantitatively characterize and model the associated transport coefficients that will be part of future studies. These studies should provide greater insight into the apparent lack of diffusion of Au to the surface and the nonuniform distribution within the film despite the long-range transport observed during irradiation seen in this initial observation.

More broadly, further work addressing the stability of the nanostructure under irradiation conditions should focus on elucidating the variations of active mechanisms through a combined effort from *in situ* work and computational modelling in a variety of ideal and commercially relevant alloy systems. As was observed at elevated temperatures in [25], segregation of Au differs based on the type of grain boundary. The effect of grain boundary character also requires more scrutiny to determine its role in nanocrystalline stability and transport. Finally, other mechanical stressors including monotonic tensile loading [22] and cyclic fatigue loading [30] have been shown to drive grain growth in nanocrystalline Pt films while showing limited or no grain growth in the Pt-10Au films. Additionally, Au is found to strengthen the material as well as improve its fatigue resistance, although the addition of Au was found to cause embrittlement [22, 30]. Future

comparison of the response of the Pt-10Au film under irradiation with the response to thermal and mechanical loading stimuli may help elucidate how coupled or sequential irradiation affects the stabilization effects of Au segregation would be interesting.

The observations in this study suggest that the philosophy of solute segregation that has been shown to improve the thermal stability of nanocrystalline materials [9-11] may not apply to the irradiation stability due to the increased complexity of intermixing associated with the cascade damage and the self-interstitial atoms being introduced. Further studies are needed to determine how broadly such differences between thermal and radiation stability are prevalent. In addition, other strategies such as tailoring grain boundary character and the addition of radiation tolerant precipitates in nanocrystalline systems may avoid such radiation induced diffusion concerns. The fundamental understanding of grain boundaries learned in model systems such as the PtAu system can assist in the development of commercially relevant alloys with advanced properties [37].

Conclusion

The beneficial properties associated with a nanocrystalline metals has largely been limited by grain boundary instability. Solute segregation has provided one effective strategy for limiting or stopping grain growth under thermal and mechanical stressors. In contrast, our results show that under irradiation conditions, solute segregation fails to limit grain growth at both room temperature and elevated temperatures Our findings suggest that irradiation induced desegregation of Au at grain boundaries defeats the stabilization mechanisms that would normally operate under purely thermal or mechanical stressors. Importantly, this study reveals that stabilization of nanocrystalline grains under one stressor does not equate to other stressors. In fact, different stressors should be explored to better understand nanocrystalline stabilization. The stabilization effects of segregated Au at the grain boundaries appear to disappear due to possible ion beam mixing. Further

investigation into the sensitivity of both the initial segregation and ion-induced desegregation on grain boundary character would provide further insight into the local mechanisms controlling nanocrystalline stabilization.

Acknowledgements

The authors thank Drs. S.M. Foiles, D. Monti, J.E. Nathaniel II, R. Dingreville, B. L. Boyce, P. Bellon, C. Daniels, and Mr. D.L. Buller, for helpful discussions and assistance. R.S., C.M.B., D.L.M., and K.H. are supported at Sandia National Laboratories by the United States (U.S.) Department of Energy (DOE) Office of Basic Energy Sciences (BES), Materials Science and Engineering Division. F. A. and Y. M. were supported through the U.S. Department of Energy, Office of Basic Energy Sciences, Materials Science and Engineering Division under Award No. DE-SC0022980. This work was performed, in part, at the Center for Integrated Nanotechnologies, an Office of Science User Facility operated for the U.S. Department of Energy (DOE) Office of Science. Sandia National Laboratories is a multimission laboratory managed and operated by National Technology & Engineering Solutions of Sandia, LLC, a wholly owned subsidiary of Honeywell International, Inc., for the U.S. DOE's National Nuclear Security Administration under contract DE-NA-0003525. The views expressed in the article do not necessarily represent the views of the U.S. DOE or the United States Government.

Author Contributions

Ryan Schoell: Data Curation, Formal Analysis, Investigation, Visualization, Writing – Original Draft Preparation, Writing – Review & Editing

Chris Barr: Conceptualization, Data Curation, Formal Analysis, Investigation, Methodology, Visualization, Writing – Review & Editing

Douglas Medlin: Data Curation, Formal Analysis, Investigation, Visualization, Writing – Reviewing & Editing

Dave Adams: Resources, Writing – Review & Editing

Yasir Mahmood: Formal Analysis, Software, Writing – Review & Editing

Fadi Abdeljawad: Formal Analysis, Software, Writing – Original Draft Preparation, Writing – Review & Editing

Khalid Hattar: Conceptualization, Funding Acquisition, Methodology, Project Administration, Resources, Supervision, Writing – Original Draft Preparation, Writing – Review & Editing

Conflict of Interest

No conflict of interest exists.

Data and Code Availability

Not Applicable

Supplementary Information

Not Applicable

Ethical Approval

Not Applicable

References:

[1]H Ni, J Zhu, Z Wang, H Lv, Y Su, X Zhang (2019) A brief overview on grain growth of bulk electrodeposited nanocrystalline nickel and nickel-iron alloys, Reviews on Advanced Materials Science 58: 98-106.
[2]D Bufford, F Abdeljawad, S Foiles, K Hattar (2015) Unraveling irradiation induced grain growth with in situ transmission electron microscopy and coordinated modeling, Applied Physics Letters 107: 191901. 1-5
[3]A Bhattacharya, Y-F Shen, CM Hefferan, et al. (2021) Grain boundary velocity and curvature are not correlated in Ni polycrystals, Science 374: 189-193.
[4]A Haslam, S Phillpot, D Wolf, D Moldovan, H Gleiter (2001) Mechanisms of grain growth in nanocrystalline fcc metals by molecular-dynamics simulation, Materials Science and Engineering: A 318: 293-312.
[5]EM Zielinski, R Vinci, J Bravman (1995) The influence of strain energy on abnormal grain growth in copper thin films, Applied Physics Letters 67: 1078-1080.
[6]J Sharon, P Su, F Prinz, K Hemker (2011) Stress-driven grain growth in nanocrystalline Pt thin films, Scripta Materialia 64: 25-28.
[7]X Zhang, K Hattar, Y Chen, et al. (2018) Radiation damage in nanostructured materials, Progress in Materials Science 96: 217-321.
[8]HA Murdoch, CA Schuh (2013) Estimation of grain boundary segregation enthalpy and its role in stable nanocrystalline alloy design, Journal of Materials Research 28: 2154-2163.

[9]JR Trelewicz, CA Schuh (2009) Grain boundary segregation and thermodynamically stable binary nanocrystalline alloys, Physical Review B 79: 094112. 1-13
[10]H Peng, M Gong, Y Chen, F Liu (2017) Thermal stability of nanocrystalline materials: thermodynamics and kinetics, International materials reviews 62: 303-333.
[11]JD Schuler, TJ Rupert (2017) Materials selection rules for amorphous complexion formation in binary metallic alloys, Acta Materialia 140: 196-205.
[12]BK VanLeeuwen, KA Darling, CC Koch, RO Scattergood, BG Butler (2010) Thermal stability of nanocrystalline Pd81Zr19, Acta Materialia 58: 4292-4297.
[13]HA Atwater, CV Thompson, HI Smith (1988) Ion-bombardment-enhanced grain growth in germanium, silicon, and gold thin films, Journal of Applied Physics 64: 2337-2353.
[14]DE Alexander, GS Was (1993) Thermal-spike treatment of ion-induced grain growth: Theory and experimental comparison, Physical Review B 47: 2983-2994.
[15]D Kaoumi, A Motta, R Birtcher (2008) A thermal spike model of grain growth under irradiation, Journal of Applied Physics 104: 073525. 1-13
[16]J Weissmüller (1994) Alloy thermodynamics in nanostructures, Journal of Materials Research 9: 4-7.
[17]SN Mathaudhu (2020) Building on gleiter: the foundations and future of deformation processing of nanocrystalline metals, Metallurgical and Materials Transactions A 51: 6020-6044.
[18]M Saber, CC Koch, RO Scattergood (2015) Thermodynamic grain size stabilization models: An overview, Materials Research Letters 3: 65-75.
[19]JW Cahn, JE Taylor (2004) A unified approach to motion of grain boundaries, relative tangential translation along grain boundaries, and grain rotation, Acta Materialia 52: 4887-4898.
[20]Y Zhang, MA Tunes, ML Crespillo, et al. (2019) Thermal stability and irradiation response of nanocrystalline CoCrCuFeNi high-entropy alloy, Nanotechnology 30: 294004. 1-15
[21]O El-Atwani, N Li, M Li, et al. (2019) Outstanding radiation resistance of tungsten-based high-entropy alloys, Science advances 5: eaav2002. 1-15
[22]WS Cunningham, K Hattar, Y Zhu, DJ Edwards, JR Trelewicz (2021) Suppressing irradiation induced grain growth and defect accumulation in nanocrystalline tungsten through grain boundary doping, Acta Materialia 206: 116629. 1-12
[23]CM Barr, O El-Atwani, D Kaoumi, K Hattar (2019) Interplay between grain boundaries and radiation damage, JOM 71: 1233-1244.
[24]RA Enrique, K Nordlund, RS Averback, P Bellon (2003) Simulations of dynamical stabilization of Ag–Cu nanocomposites by ion-beam processing, Journal of Applied Physics 93: 2917-2923. Doi:10.1063/1.1540743
[25]X Zhang, S Shu, P Bellon, RS Averback (2015) Precipitate stability in Cu–Ag–W system under high-temperature irradiation, Acta Materialia 97: 348-356.
[26]RA Enrique, P Bellon (2001) Self-organized Cu–Ag nanocomposites synthesized by intermediate temperature ion-beam mixing, Applied Physics Letters 78: 4178-4180. Doi:10.1063/1.1379358
[27]J Monti, E Hopkins, K Hattar, F Abdeljawad, B Boyce, R Dingreville (2022) Stability of immiscible nanocrystalline alloys in compositional and thermal fields, Acta Materialia 226: 117620. 1-19
[28]P Lu, F Abdeljawad, M Rodriguez, et al. (2019) On the thermal stability and grain boundary segregation in nanocrystalline PtAu alloys, Materialia 6: 100298. 1-9
[29]NM Heckman, SM Foiles, CJ O'Brien, et al. (2018) New nanoscale toughening mechanisms mitigate embrittlement in binary nanocrystalline alloys, Nanoscale 10: 21231-21243.

[30]CM Barr, SM Foiles, M Alkayyali, et al. (2021) The role of grain boundary character in solute segregation and thermal stability of nanocrystalline Pt–Au, Nanoscale 13: 3552-3563.
[31]MDZ J. F. Ziegler, J.P. Biersack, E. Dabich, H. Paul, D. J. Marwick, G. A. Cuomo, W. A. Porter (2008), Stopping Range of Ions in Matter
[32]C O'Brien, C Barr, P Price, K Hattar, S Foiles (2018) Grain boundary phase transformations in PtAu and relevance to thermal stabilization of bulk nanocrystalline metals, Journal of Materials Science 53: 2911-2927.
[33]EA Holm, SM Foiles (2010) How grain growth stops: A mechanism for grain-growth stagnation in pure materials, Science 328: 1138-1141.
[34]K Nordlund, R Averback (1999) Inverse Kirkendall mixing in collision cascades, Physical Review B 59: 20-23
[35]ML Crespillo, JT Graham, Y Zhang, WJ Weber (2016) Temperature measurements during high flux ion beam irradiations, Review of Scientific Instruments 87: 024902. 1-7
[36]J Piochaud, M Nastar, F Soisson, L Thuinet, A Legris (2016) Atomic-based phase-field method for the modeling of radiation induced segregation in Fe–Cr, Computational Materials Science 122: 249-262.
[37]C Du, S Jin, Y Fang, et al. (2018) Ultrastrong nanocrystalline steel with exceptional thermal stability and radiation tolerance, Nature Communications 9: 5389. 1-9 Doi:10.1038/s41467-018-07712-x